Research Article
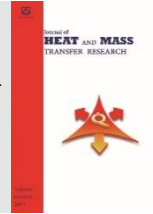
Numerical Assessment and Data-Driven Reduced Order Model for Natural Convection of Water-Copper Nanofluid in Porous Media

Mohammad Kazem Moayyedi *, a, b (iD)

a CFD, Turbulence, and Combustion Research Laboratory, Department of Mechanical Engineering, University of Qom, Iran.
b Institute of Aerospace Studies, University of Qom, Iran.

PAPER INFO

ABSTRACT

In this article, two computational frameworks are presented for the numerical simulation of flow and heat transfer under the effects of natural convection phenomena in a field containing water-copper Nano-fluid and including porous media. The first is a CFD model which is built based on accurate algorithms for spatial derivatives and time integration. The spatial derivatives have been calculated using first-order upwind and second-order central differencing approaches. Also, time integration is performed using the fourth-order Runge-Kutta method. In the second, a parametric reduced order model is developed to compute the whole flow field under the effects of some important parameters such as Darcy number and Rayleigh number. This model is constructed based on POD-snapshots method. The POD modes are calculated by the solution of an eigenvalues problem. The calculated eigenfunctions are POD modes which are ranked using energy-based criteria based on the total kinetic energy of the flow field. This approach leads to the development of a reduced-order model that can be used as a surrogate model of the CFD high-order approach. The results obtained from the reduced order model show relatively good agreements under variations of some important parameters such as Darcy and Rayleigh numbers and nanoparticles density on the flow and thermal fields with the benchmark DNS data. Also, from the results, it is concluded that the surrogate model has very small values of errors (order of $10^{-4} \sim 10^{-6}$) and the time spent on calculations is less than 10% of the time required for direct numerical simulation.

1. Introduction

The buoyancy driven convective motions is reputable natural phenomena, and has many attention in different research works. The Study of natural convection in enclosures filled with Nanofluids have been studied extensively for various geometries and problem statements in the last few years. The heat transfer enhancement in a differentially heated enclosure based on variable thermal conductivity and variable viscosity of Al2O3–water and CuO–water nanofluids investigated by Abu-Nada et al. [1]. Bouhalleb and Abbasi investigated heat transfer, and fluid flow of natural convection in an inclined cavity filled with CuO-water Nanofluid heated from one side and cooled from the ceiling[2]. Bishwajit Sharma et al. studied laminar flow heat transfer of Cu-water Nanofluid inside a square cavity using the numerical approach. The cavity is heated by different length heaters with isothermal boundary condition placed symmetrically on two adjacent sides[3]. Izadi and his

Corresponding Author: Mohammad Kazem Moayyedi.
Email: moayyedi@qom.ac.ir

colleagues studied the natural convection of multi-wall carbon nanotubes-Iron Oxide nanoparticles/water hybrid nanofluid inside the specifically shaped enclosure using Lattice Boltzmann Method [4]. The effects of inclination angle and nanoparticle concentration on mixed convection of a lid-driven cavity that is filled by Al2O3/water nanofluid were investigated by Izadi [5]. Izadi et al. studied the modeling of effective thermal conductivity and viscosity of carbon-structured nanofluids [6]. Izadi and his colleagues numerically investigated laminar forced convection of a nanofluid flowing in a duct at microscale [7]. Izadi et al. studied forced convection heat transfer of TiO2/water nanofluid flow inside a double-pipe heat exchanger with spindle-shaped turbulators [8]. Thermal and flow behaviors of sensible heat energy storage unit subjected to uniform and nonuniform magnetic field effects magnetic field effects and to double time dependent heat sources were numerically investigated by Izadi [9]. Nazia et al. investigated the mass and heat transport of silver–ethylene glycol and copper–EG-based nanofluids between two rotating stretchable disks under convective boundary conditions [10]. Reddy analyzed modified Fourier heat flux on flow and heat transfer characteristics of magnetic nanofluid inside a cavity packed with Ethylene Glycol-Multiwalled carbon nanotubes type nanofluid by taking thermal radiation [11]. Aminian et al. studied numerically flow and heat transfer characteristics of CuO/H2O nanofluid within a mini tube [12].

The buoyancy driven phenomena in porous media is one the most attractive area which is actively under investigation. Non-Darcy natural convection in porous media has received a great deal of consideration recently due to applications in fluid flow in geothermal reservoirs, dispersion of chemical contaminants through water saturated soil, migration of moisture in grain storage system, crude oil production[13-14]. Bourantas et al. investigated the natural convection of a nanofluid in a square cavity filled with a porous matrix using a meshless technique. The Darcy–Brinkman and the energy transport equations were been used to model the nanofluid flow and the heat transfer process in the porous medium as these are generated by heating one of the cavity walls[15]. Prabir Barman and his colleagues used a numerical approach to study the natural convection on the buoyancy-driven flow of nanofluids and heat transfer through porous media packed inside a wavy cavity. The cavity is placed horizontally, and its right vertical wall is of wavy nature, the bottom and top walls of the cavity are adiabatic[16]. Basil Mahdi Al-Srayyih et al. studied the buoyancy-driven flow inside an enclosure filled with composite porous-hybrid nanofluid layers using a numerical method based on a local thermal nonequilibrium model for the heat transfer between the fluid and the solid phases. The bottom wall of the enclosure was partly heated to provide a heat flux, while the other parts of the wall were adiabatic. The top and vertical walls of the enclosure were maintained at constant cold temperatures. They used the Darcy-Brinkman model to model the flow inside the porous layer [17]. Zehba A. S. Raizah studied the natural convection flow resulting from heat partitions in an H-shaped enclosure filled with a nanofluid using an incompressible smoothed particle hydrodynamics (ISPH) method. The right area of the H-shaped enclosure is saturated with non-Darcy porous media [18]. Mehryan et al. investigated the natural convection of Ag-MgO/water nanofluids within a porous enclosure using a Local Thermal Non-Equilibrium (LTNE) model [19]. Izadi studied the impact of porous materials, nano-particle types, and their concentrations on transient natural convection heat transfer of nano-fluid inside a porous chamber with a triangular section [20]. A computational investigation of transient thermogravitational energy transport in H2O/Al2O3 nanoliquid and water-based copper/aluminum oxide hybrid nanofluid (water/Al2O3-Cu) inside a horizontal isosceles triangular enclosure with the porous medium was performed by Izadi et al. [21]. Sajjadi et al. studied the natural convection flow in a porous cavity with sinusoidal temperature distribution by a new double multi relaxation time (MRT) Lattice Boltzmann method [22]. Izadi et al. studied numerically the natural convective heat transfer of a magnetic nanofluid in a porous medium subjected to two variable magnetic sources [23]. The flow and heat transfer characteristics of Cu/water nanofluid in a semi-circular cavity are analyzed by Izadi el al. [24].

The reduced order models (ROMs) have prepared new bases for the fast computation of engineering problems. These models are containing two primary forms, one is called pure data-driven frameworks which are operated as parametric reduced order models. In the second kind, the model has been obtained by combination of data which are obtained from dynamical system responses and the conservation laws and is called the intrusive reduced order model. The ROMs prepare an appropriate foundation to coupling the different dynamical systems and they make the surrogate frameworks for researchers and engineers to test and validate their new ideas and experiments. The intrusive ROMs contain two types of errors, one from the projection and the second due to the modeling and the integration. The first type of error, refers to the projection procedure, for example, the snapshots resolution. The second type of error is due to some assumptions which are used to construct the reduced order model. Proper orthogonal Decomposition (POD) is one of the most common dimensionality reduction methods, that is a linear and unsupervised scheme. To do calculations quickly and simply, POD reduces the

dimensions of data [25]. The proper orthogonal decomposition generates an orthogonal n-dimensional coordinate system that provides a more accurate approximation than other orthogonal n-dimensional coordinate systems, which are used to describe a set of snapshots from the assumed area [26]. Karhunen-Loeve first proposed this method for analyzing the statistical data [27]. Holmes used this method for extracting large scale structures of turbulent flows [28]. A historical review of POD was presented by Luciaa et al. [29]. Smith used POD for simulation of turbulent flow as a reduced order model [30].

The method of snapshots, which is introduced by Sirovich, is a useful tool to develop reduced order models for complex dynamical systems that some data from their response from either experimental tests or direct numerical simulation are available [31]. Because of the ability of POD in extracting the high-level energy modes, this method can be used for coupled dynamical system modelling such as fluid-structure interaction [32], multiphase flow [33], and optimal control problems [34-35]. Studying the physics of turbulent flow inside an open channel [36], modeling the supersonic, transonic, and subsonic flow around an airfoil, and inverse design of aerodynamics shapes is also other applications of this approach [37, 38, 39]. A POD-based reduced order stabilized mixed finite volume element (SM-FVE) extrapolating model has been established with very few degrees of freedom for the non-stationary incompressible Boussinesq equations[40].

In this research, the mathematical formulation of the modified version of the Navier-Stokes equations for the simulation of nanofluid in porous media is presented. In the next section, a well-validated computational approach for the spatial and temporal terms will be introduced. Also, the basic theory of the POD-snapshots method and the developed reduced order framework to model the fluid flow and thermal field are explained.

In the final section, the results of the proposed model and a comparison with the CFD simulations will be presented. Based on the literature review, the development of a surrogate model for the simulation of natural convection of nano-fluid in porous media considering a data-driven approach has not been studied yet. The aim of this research is focused to build up a parametric reduced order model which can simulate this kind of nano-fluid problem.

2. Governing Equations

The governing equations of fluid flow contain continuity, Darcy–Brinkman and energy transport equations with a term due to the effects of temperature gradients (Boussinesq approximation) as follow[14]:

$$\nabla \cdot \mathbf{u} = 0$$

$$\frac{\partial u}{\partial t} + (\mathbf{u}.\nabla)u = \frac{\varepsilon}{\rho_{nf}}(-\frac{\partial p}{\partial x} + \mu_{nf}\nabla^2 u) - \frac{\mu_D \varepsilon^2}{\rho_{nf} K}u$$

$$\frac{\partial v}{\partial t} + (\mathbf{u}.\nabla)v = \frac{\varepsilon}{\rho_{nf}}(-\frac{\partial p}{\partial y} + \mu_{nf}\nabla^2 v)$$
$$- \frac{\mu_D \varepsilon^2}{\rho_{nf} K}v + \varepsilon^2 \beta_{nf} g(T - T_c) \tag{1}$$

The continuity and momentum equations can be expressed in vorticity-stream function form:

$$\nabla^2 \psi = -\omega$$

$$\frac{\partial \omega}{\partial t} + (\mathbf{u}.\nabla)\omega = \varepsilon \frac{\rho_f}{\rho_{nf}} \frac{\mu_{nf}}{\mu_f} \Pr \nabla^2 \omega$$
$$- \varepsilon^2 \frac{\Pr}{\mathrm{Da}} \frac{\rho_f}{\rho_{nf}} \frac{\mu_{nf}}{\mu_f} \omega + \varepsilon^2 \frac{\beta_{nf}}{\beta_f} \mathrm{Ra}\,\Pr \frac{\partial \tilde{T}}{\partial x} \tag{2}$$

where, *Pr* is Prandtl number, *Da* is Darcy number and *Ra* is Rayleigh number which are defined as:

$$\mathrm{Da} = \frac{K}{L^2}, \qquad\qquad \Pr = \frac{\nu_f}{\alpha_f},$$

$$\mathrm{Ra} = \frac{g \times \beta \times \Delta T \times L^3}{\nu_f \times \alpha_f}$$

ε is porosity coefficient, the energy transport equation is as [15]:

$$\frac{\partial \tilde{T}}{\partial t} + (\mathbf{u}.\nabla)\tilde{T} = \frac{k_{nf}}{k_f} \frac{\rho C_{p\,f}}{\rho C_{p\,nf}} \nabla^2 \tilde{T} \tag{3}$$

The heat capacity of the nanofluid is calculated using the density ratio of nanoparticles, φ as [15]:

$$\rho C_{p\,nf} = (1 - \varphi)\ \rho C_{p\,f} + \varphi\ \rho C_{p\,p} \tag{4}$$

The thermophysical properties of the base fluid and the copper nanoparticles are given in Table 1:

Table 1. Thermophysical Properties of Water and Copper [15]

	Water	Copper
$\rho(\mathrm{kg}/\mathrm{m}^3)$	997	8933
$C_p(\mathrm{J}/\mathrm{kg\,K})$	4179	385
$k(\mathrm{W}/\mathrm{m\,K})$	0.613	400
$\beta(1/\mathrm{K})$	2.1×10⁻⁴	1.67×10⁻⁵

3. Numerical Schemes

The governing equations are discretized in both time and space and then used pseudo-time marching approach to solve them (except for the stream-function equation). For the stream-function equation used a conventional iterative solution method for elliptic equations (Such as the SOR algorithm in explicit or implicit form).

3.1. Spatial Discretization

The convective terms of the vorticity transport and energy conservation equations are discretized using an upwind Riemann variable method based on the sign of the velocity vector, as [41]:

$$uu_x = a_{ij}^+ u_x^- + a_{ij}^- u_x^+$$

$$u_x^- = \frac{u_{i,j} - u_{i-1,j}}{\Delta x} \qquad u_x^+ = \frac{u_{i+1,j} - u_{i,j}}{\Delta x} \qquad (5)$$

$$a_{i,j}^- = \min(u_{i,j}, 0) \qquad a_{i,j}^+ = \max(u_{i,j}, 0)$$

The central difference formulation for the interior nodes of the computational domain is as follows:

$$\frac{\partial F}{\partial x} = \frac{F_{i+1,j} - F_{i-1,j}}{2\Delta x} \qquad (6)$$

for the points on the boundaries, a forward or backward second-order differential formula is used as follows:

$$\frac{\partial F}{\partial x} = \frac{-3F_{i,j} + 4F_{i+1,j} - F_{i+2,j}}{2\Delta x}$$

$$\frac{\partial F}{\partial x} = \frac{3F_{i,j} - 4F_{i-1,j} + F_{i-2,j}}{2\Delta x} \qquad (7)$$

Also, diffusion terms have been discretized using a second-order finite difference method:

$$\frac{\partial^2 F}{\partial x^2} = \frac{F_{i+1,j} - 2F_{i,j} + F_{i-1,j}}{\Delta x^2} \qquad (8)$$

3.2. Time Integration

Time discretization of transport equations is performed using the fourth-order Explicit Runge-Kutta method. This method is a convenient and accurate way for time integration of the unsteady or steady flows governing equations [41].

4. Proper Orthogonal Decomposition

The POD Reduced-order modelling begins by finding the empirical eigenfunctions using the Karhunen-Loève decomposition. Then the flow variables are approximated using expansions of these eigenmodes. POD is remarkable in that the selection of basis functions is not just appropriate, but optimal is described further in the analysis section. POD was introduced to the turbulence community by Lumley in 1967. Before that, it was already known in statistics as the Karhunen-Loève expansion. Lumley proposed that a coherent structure can be defined with functions of the spatial variables that have maximum energy content. That is, coherent structures are linear combinations of which maximize the following expression [28]:

$$max \frac{\left\langle \phi, u^{2} \right\rangle}{\left\langle \phi, \phi \right\rangle} \qquad (9)$$

where, ϕ, u is the inner product of the basis vector ϕ with the field, u. Note $\langle \cdot \rangle$ is the time-averaging operation. It can be shown that the POD basis vectors are eigenfunctions of the Kernel $\mathbf{K}$, given by[28]:

$$\mathbf{K} = \left\langle u, u'^{2} \right\rangle \qquad (10)$$

where u' denotes the Hermitian of u. This equation is converted to the Fredholm's second kind integral equation, and its discretization leads to an eigenvalue problem. In this work, the SVD method has been used to solve this eigenvalue problem [37].

If equation (9) was maximized, the projected field along with $\phi(x)$, has a larger amount average energy than any other reconstructions along with other basis functions. POD eigenfunctions are defined as eigenvectors of space correlation tensor. Approximation of this tensor is very difficult but using the POD snapshot method, it becomes easier to do. For this purpose, an ensemble of fluctuations, $u_n(x)$, with *N* members in different time steps or other variable changes will be needed. It can be obtained from CFD simulations or experimental tests as follow:

$$u_n(x) = u(x, t^n) \qquad (11)$$

t^n is a variable which can belong to parameters of time or any effective parameters. By using flow field modes, it can be reconstructed by the following relation [39]:

$$u(x, t) = \sum_{j=1}^{N} a^j(t) \phi^j(x) \qquad (12)$$

4.1. Data-Driven Model based on Proper Orthogonal Decomposition

Generally, in a POD analysis, variations of any selected quantities of the flow field, in the form of a matrix of numerical data for different some important parameters, separately, are considered as initial data. This parameter can be an arbitrary parameter, δ, such as Rayleigh number, Darcy number, or etc. To predict the flow field for each value of δ, should collect a set of numerical data of the flow field for different valuesof δ, which is arranged, intentionally. Then an eigenvalue problem should be solved. Now, ϕ^j, are eigenvalues of this matrix which is also called the flow field modes. To reconstruct the field for any desired value of δ, the modal coefficients (a^j) should be interpolated. Now, the field can be reconstructed using equation (10). Given a tabulated function $y_i = y(x_i)$, i=1,...,N, focus attention on one particular interval, between x_j and x_{j+1}. Linear interpolation in that interval gives the interpolation formula:

$$y = Ay_j + By_{j-1}$$

$$B = \frac{x_j - x}{x_{j+1} - x_j} \qquad A = \frac{x_{j+1} - x}{x_{j+1} - x_j} \qquad (13)$$

Equation (13) is a special case of the general Lagrange interpolation formula. Since it is (piecewise) linear, equation (13) has zero second derivative in the interior of each interval, and an undefined, or infinite, second derivative at the abscissas x_j. The goal of cubic spline interpolation is to get an interpolation formula that is smooth in the first derivative, and continuous in the second derivative, both within an interval and at its boundaries [39].

4.2. Order Reduction Strategy

Normally, when the number of modes is increased, the reconstruction is performed with the better accuracy. It is required to use the optimal number of modes for data reconstruction. This is equivalent to capturing the highest level of the energy and the least number of modes for model construction (Figure 10). In this manner, a fraction number is defined for automatic selection of modes as follow:

$$\kappa = \left. \sum_{i=1}^{N_r} \lambda_i \middle/ \sum_{i=1}^{N} \lambda_i \right. \tag{14}$$

if κ is about 99.9%, and N_r is the optimum number of modes to construct the reduced order model[41].

5. Flow Configuration and Boundary Conditions

The problem which has been studied in this research is a square cavity with a heated plate on the bottom side and cooled walls at the left, right and top sides. Also, at the bottom side two parts are defined using adiabatic wall boundary condition. At all sides of the cavity used no slip boundary condition for velocity. This field contains water-copper Nano-fluid in a porous media. The computer code can be run for different percentages of nanoparticles in the primary fluid. Figure **1** shows the geometry and appropriate boundary conditions of the control volume. A structured rectangular mesh was used as the computational platform for the numerical solution of the flow field. The grid points are refined near to the wall faces, and it tried to maintain the quality of the mesh at the domain interior.
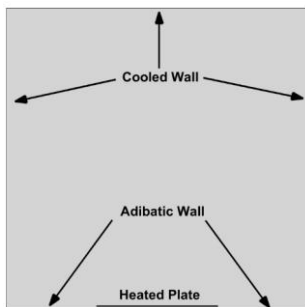

Figure 1. Geometry of and related boundary conditions of the square cavity test case.

6. Grid Independent Study

For the grid independent study, the value of the average Nusselt number on the heated plate is used. For this purpose, six different sizes of computational mesh are considered. For these mesh qualities, the flow and thermal fields are simulated under the effects of nanoparticles with a density ratio of 0.1. Also, Darcy and Rayleigh numbers are considered as 10^{-4} and 10^5 respectively. Figure **2** shows the variations of the average Nusselt number versus the total number of elements which are listed in Table **2**. It is obvious that the value of the Nusselt number shows less than a 1% difference between mesh numbers 5 and 6. Therefore, mesh number 5 has been used for all computations in this paper.

Table 2. Computational grids configuration

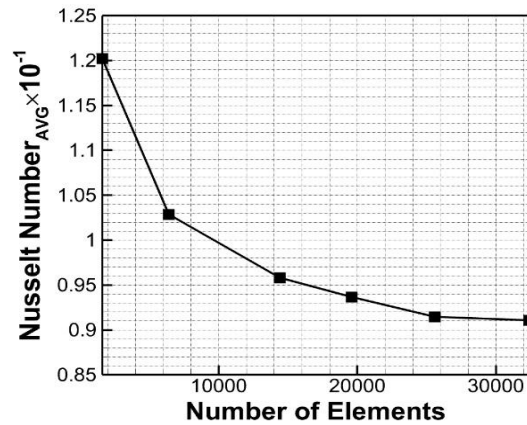|	Mesh	Total Number of Elements
1	40×40	1600
2	80×80	6400
3	120×120	14400
4	140×140	19600
5	160×160	25600
6	180×180	32800

Figure 2. Variations of average Nusselt number on the heated plate versus total number of elements.

7. CFD Model Validation

To verify the accuracy of the computer code used to generate the snapshots for training the reduced order model, its results compared with suitable benchmark data. For this purpose, a simulation was performed for $Ra=10^5$, $Da=10^{-4}$, $\varepsilon=0.4$, and $\varphi=0.1$. In Fig. **3**, distribution of dimensionless temperature along the horizontal line at the mid height of the cavity has been shown. Figure **4** shows dimensionless temperature variation along x-direction at y=0.1. Distribution of temperature in vertical direction at x=0.5 is also shown in Fig. **5**. It is clear the obtained results of the present study have good agreement with the related benchmark results.
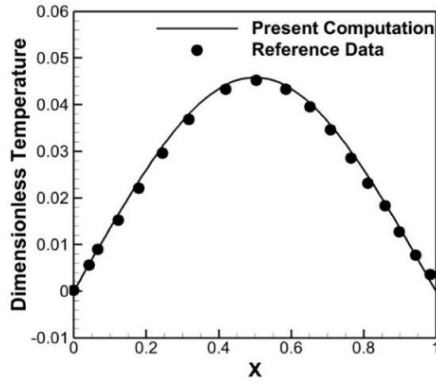
Figure 3. Comparison of temperature variations at y=0.5 between present study and reference data [15].
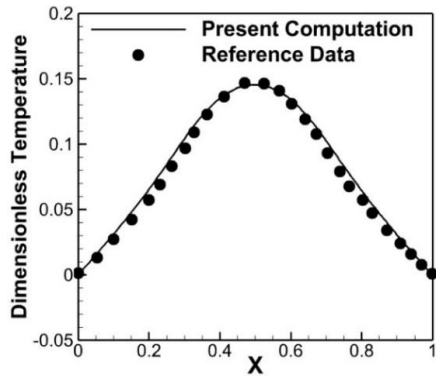

Figure 4. Comparison of temperature variations at y=0.1 between present study and reference data [15].
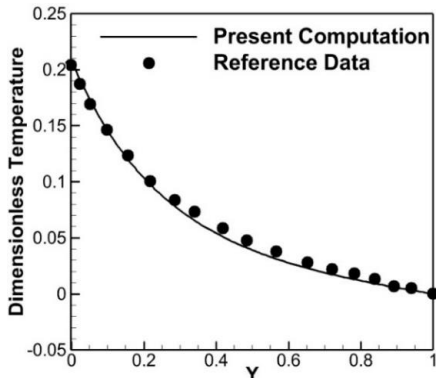

Figure 5. Comparison of temperature variations at x=0.5 between present study and reference data [15].

8. Results and Discussion

In this section, the results of this research will be presented and discussed them. The results contain two parts, in the first, the outcomes of flow field simulations in the field containing Nano-fluid of water copper in porous medium under the effects of natural convection have been presented. In the next section, the results of the reduced order model of this problem are exhibited. To validate the accuracy of the surrogate model, its results have been compared with the direct simulation data.

8.1. Direct Numerical Simulation

In this section, the CFD code used to simulate the entire flow field under the effects of some important parameters such as Rayleigh number, Darcy number and density ratio of nanoparticles. Figure **6** shows the distribution of local Nusselt number along the vertical centreline of the cavity at a fixed Rayleigh and Prandtl numbers and for two values of Darcy number. Both parts of this figure are illustrating the distribution of Nusselt number for different values of density ratio of nanoparticles. It can be seen that by increasing the density ratio of nanoparticles, the maximum value of the local Nusselt number is increased near the heated plate on the bottom wall which shows that the heat transfer is enhanced in different layers of the flow. Also, by increasing Darcy number the value of local Nusselt number is reduced and by moving toward the bottom wall and near the heated plate, the gradient of Nusselt number is reduced unlike the near the top wall.

Figure **7** illustrates the contours of temperature for different values of Darcy number. Also, the effect of variations of the nanoparticles density ratio on streamlines of flow has been shown in Fig. **8**.
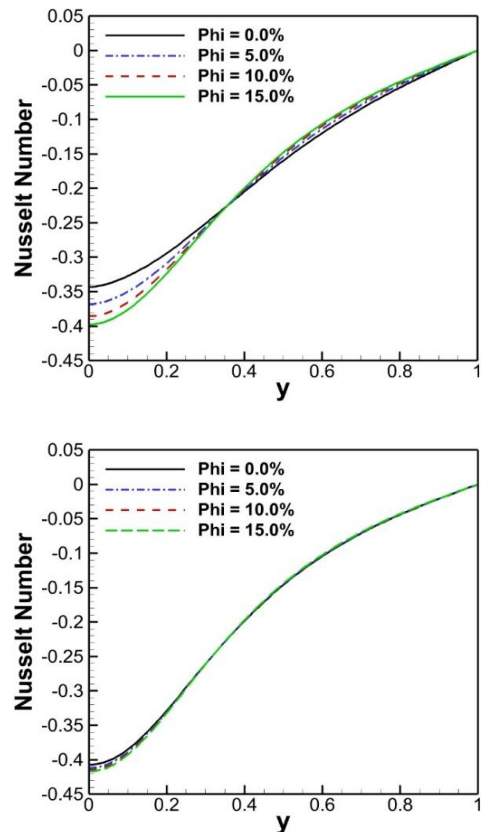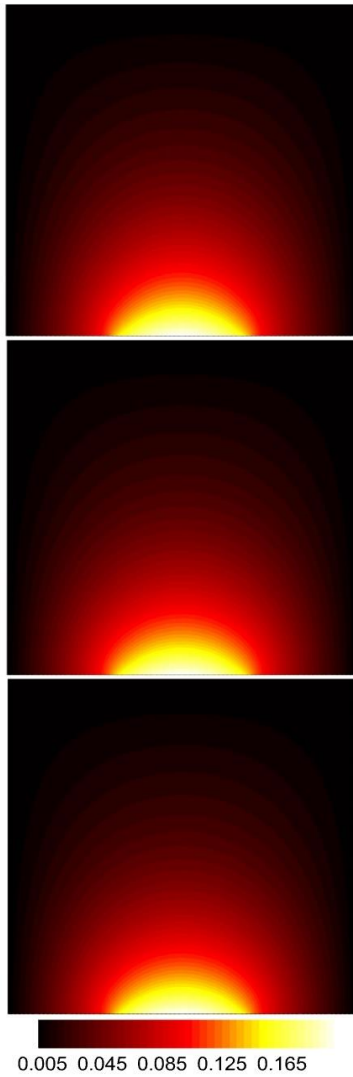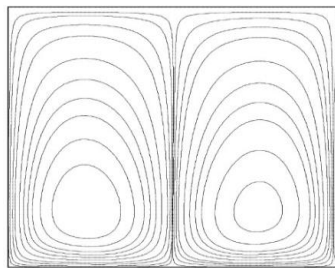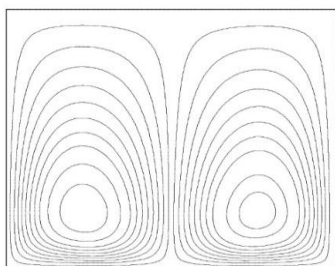

Figure 6. Distribution of local Nusselt number along the vertical centreline of the cavity at *Ra*=10^5, *Pr* = 6.2, and *Da* = 10^{-3} (Top) and *Da*=10^{-4}(Bottom) for different density rate of Nano Particles.

Figure 8. Streamlines of natural convection of water-copper nanofluid in porous media at Ra = 105, Da= 10-4, Pr= 6.2, ε = 0.4, and φ = (a) : 0.0, (b): 0.05, (c): 0.1, (d): 0.15.

8.2. Data-Driven Model for Flow and Thermal Fields

In this section, the results obtained by the surrogate reduced order model are presented. The model has been developed using three modes. The results contain the flow field and heat transfer inside a domain encompassing water copper nano-fluid and a heated horizontal plate inside porous media. Two datasets have been used to train the data-driven model, in the first, all data were obtained using different values of Darcy number. So, the second snapshots ensemble is created using various density ratio of nanoparticles. For both datasets, Rayleigh number has been considered as 10^5 and Prandtl number of 6.2.

In Table **3**, the level (percentage) of the kinetic energy (in the dimensionless form) of the first four strongest modes of the temperature field for the first dataset are shown. In the third row of the table, the total energy by adding the energy level of each new mode is listed. As it is clear, only the first two modes capture more than 99% of the kinetic energy of the entire energy of the system, while the remaining two modes only change less than 1% of the total energy.

Figure **9** shows the first three highest energy level modes of vorticity, streamfunction, and temperature for the natural convection of water-copper nanofluid in porous media field for the first dataset.
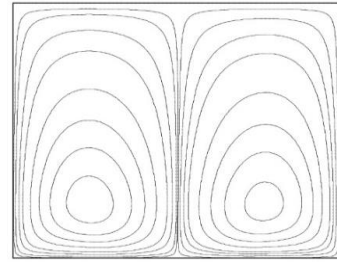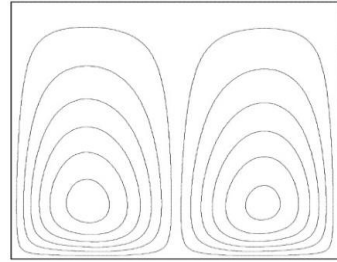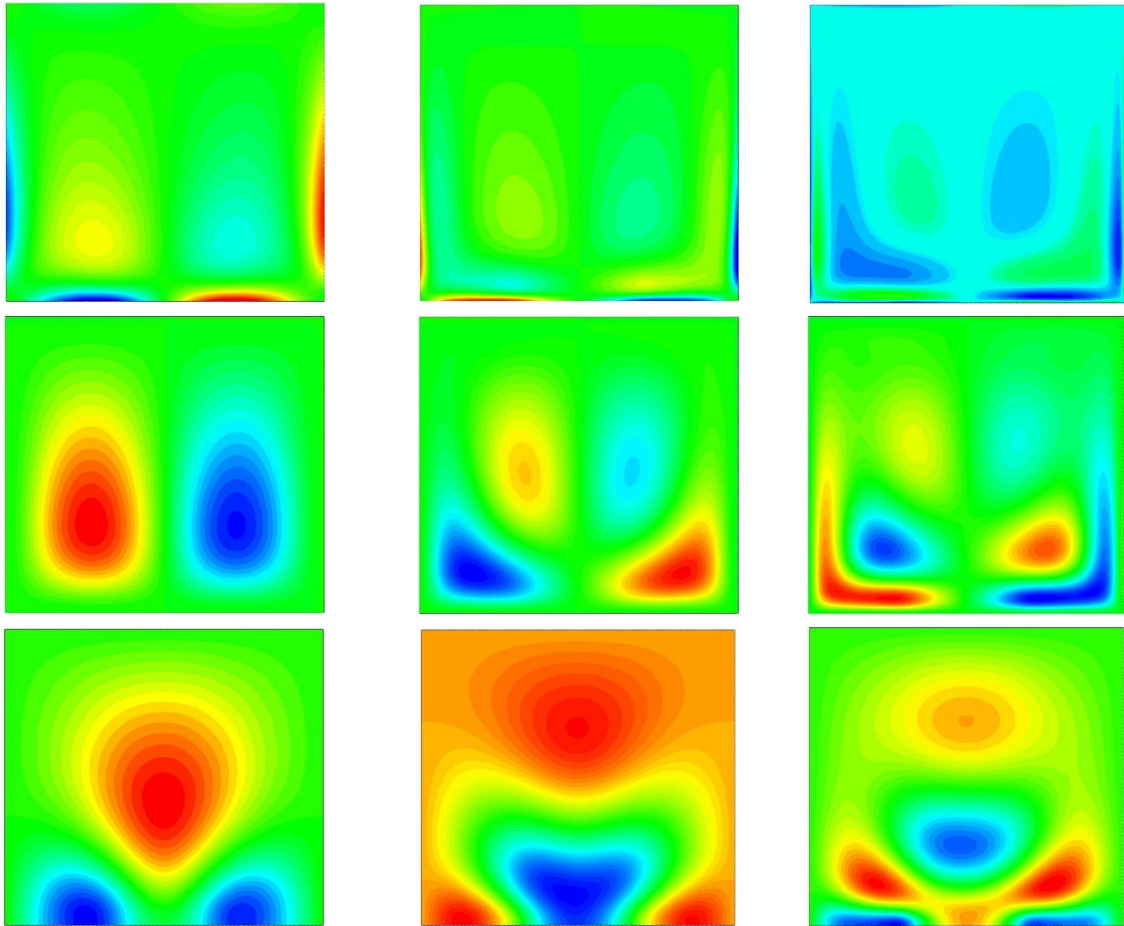

Figure 7. Contours of temperature for natural convection of water-copper Nanofluid in porous media at Ra=10⁵, *Pr*=6.2, φ = 0.1, ε = 0.4, and *Da* = 10⁻³(top) 10⁻⁴(middle) and 10⁻⁵(bottom).

Table 3. Relative energy level of the temperature field for the first dataset

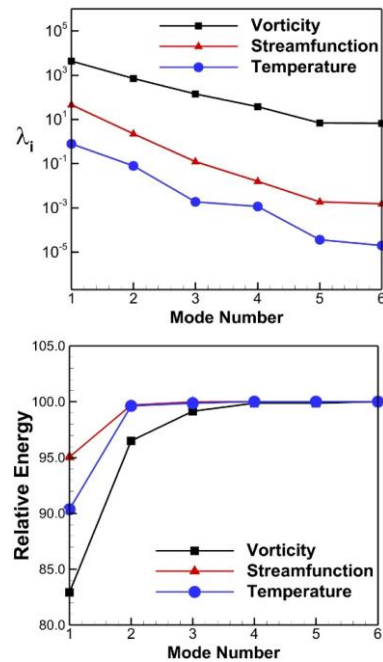| Mode Number	Energy Level	Total Energy
1	90.3%	90.3%
2	9.27%	99.64%
3	0.217%	99.86%
4	0.131%	99.99%

Figure 9. Distribution of first three strongest modes of vorticity (top), streamfunction (middle) and temperature (bottom) for natural convection of water-copper nanofluid in porous field at Ra=10^5, Pr = 6.2, φ = 0.1, ε = 0.4

Figure **10** shows the distribution of eigenvalues and relative energy of POD modes versus their index for the first dataset. From these figures, a similar trend related to table **1** which is explained about the impact level of each mode of vorticity, streamfunction and temperature, can be found.

In Fig. **11** distribution of local Nusselt number along the heated wall, which is reconstructed using CFD model and reduced order POD model, for different values of Darcy number is illustrated. It is evident from this figure that the reduced order model predicts relatively accurate results.

In table **4**, the level (percentage) of the kinetic energy of the first four strongest modes of the temperature and the total energy for adding each new mode, related to second dataset, are demonstrated. It is clear, only the first two modes capture more than 99% of the total kinetic energy of the system, while the other two modes only contain approximately 1% of the total energy.


Figure 10. Distribution of eigenvalues (top) and relative energy (bottom) versus mode number for natural convection of water-copper nanofluid in porous field at Ra=10^5, *Pr*=6.2, φ = 0.1, ε = 0.4.

Table 4. Relative energy level of the temperature field for the second dataset

Mode Number	Energy Level	Total Energy
1	99.03%	90.03%
2	0.81%	99.85%
3	0.12%	99.97%
4	0.024%	99.99%

Table 5. Relative energy level of the temperature field for the second dataset

| Mode Number	Energy Level	Total Energy
1	99.03%	90.03%
2	0.81%	99.85%
3	0.12%	99.97%
4	0.024%	99.99%
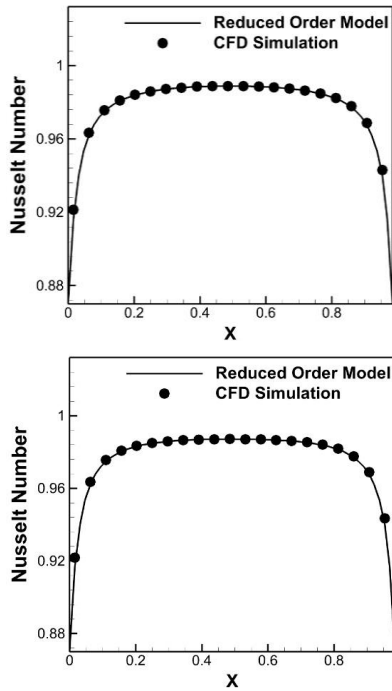
Figure 11. Comparison between the distribution of local Nusselt number along the heated wall (on bottom face) for *Da* = 3×10⁻⁴ (top) and 2×10⁻³(bottom) at Ra=10⁵, *Pr*=6.2, φ = 0.1, ε = 0.4, reduced order model (solid Line) and CFD data (points).

In Fig. **12** distribution of the first three highest energy level modes of vorticity, streamfunction and temperature for the natural convection of water-copper nanofluid in a porous media for the second dataset, is illustrated.

Figure **13** shows the distribution of eigenvalues and relative energy of POD modes versus their index for this dataset. It is obvious that the first mode of vorticity, streamfunction and temperature are very similar to the related field (instantaneous field). This is related to the main concept, which is shown in figure 10, that the first mode of these variables is the most energetic and important feature. Therefore, it can be formed as the original related flow field.

Figure **14** shows the distribution of local Nusselt number along heated wall computed using CFD high order model compared to the similar results obtained by the reduced order model. The top figure is for density ratio of nanoparticles equal to 0.03 while the bottom figure is related to the density ratio of 0.12. Both values mentioned in these results are not available in the primary snapshots of the flow field. It is obvious from these figures that the reduced order model could predict relatively accurate results.
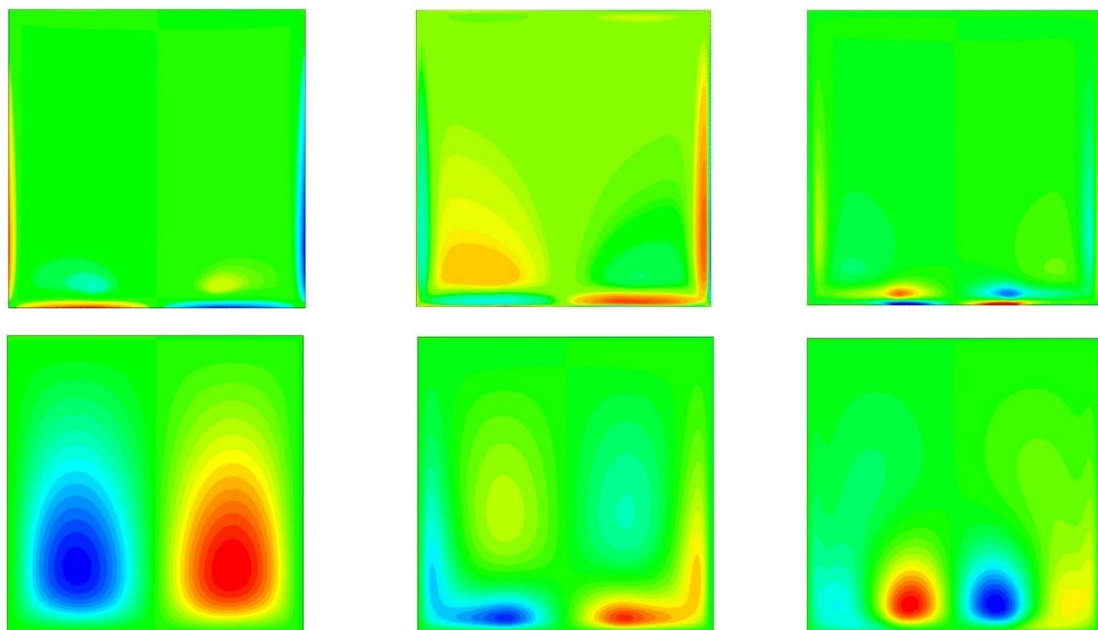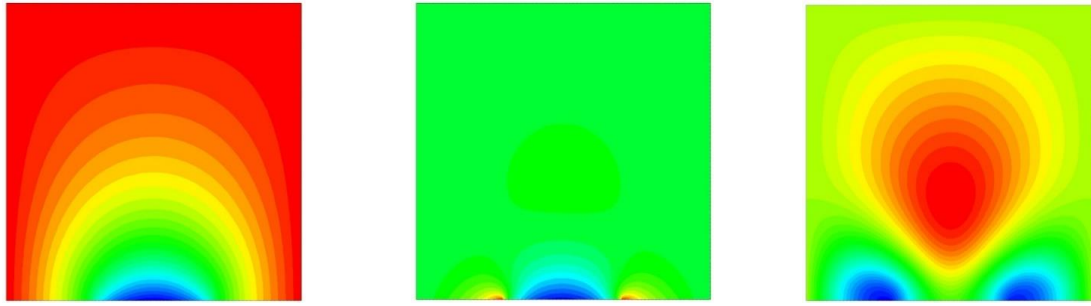
Figure 12. Distribution of first three strongest modes of vorticity (top), streamfunction (middle) and temperature (bottom) for natural convection of water-copper nanofluid in porous field at $Ra=10^5$, $Pr = 6.2$, $Da=10^{-4}$, $\varepsilon = 0.4$.
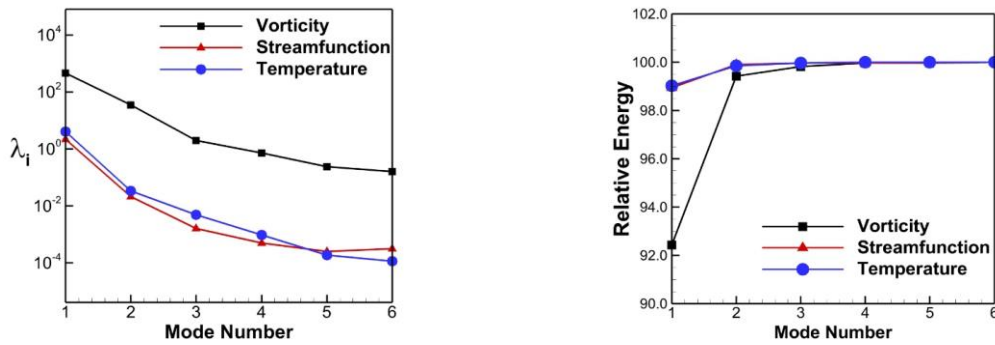

Figure 13. Distribution of eigenvalues (left) and relative energy (right) versus mode number for natural convection of water-copper nanofluid in porous field at $Ra=10^5$, $Pr = 6.2$, $Da = 10^{-4}$, $\varepsilon = 0.4$.
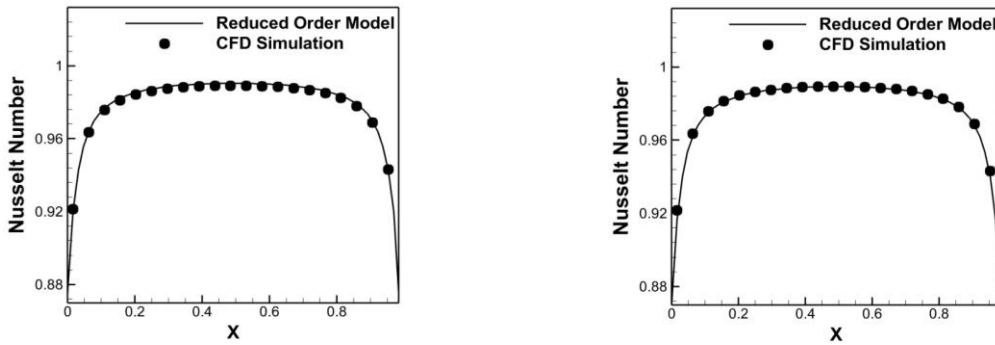

Figure 14. Comparison between the distribution of local Nusselt number along the heated wall (on bottom face) for density ratio of 0.03(top) and 0.12(bottom) at $Ra=10^5$, $Pr=6.2$, $\varphi = 0.1$, $\varepsilon = 0.4$, reduced order model(solid Line) and CFD data (points).

A comparison between contours of temperature and streamlines of the flow field obtained from the surrogate model and high order CFD model for two values of density ratio of nanoparticles is shown in Fig. **15**.

The reduced order model is developed using the second dataset. It is to be noted that the left figure is for the density ratio of nanoparticles equal to 0.03 and the right figures are related to the density ratio of 0.12. All figures prove that the results obtained from the reduced order model are in good agreement with the direct simulation results.

For a demonstration of the accuracy of the reduced order model comparing the direct simulation results,

the root mean square error for the whole domain has been calculated by the following equation [42]:

$$RMSE = \sqrt{\frac{\sum_{i=1}^{N} \left| f_i^{CFD} - f_i^{ROM} \right|^2}{N}} \qquad (15)$$

Table **5** shows the values of RMSE for different flow field variables such as temperature, streamfunction, and vorticity by considering two values of nanoparticles density ratio of 0.03 and 0.12. It is obvious that the results obtained by ROM in the whole domain have less relative error comparing the CFD data for all three important variables of the considered problem.

(a)

(b)

(c)

(d)
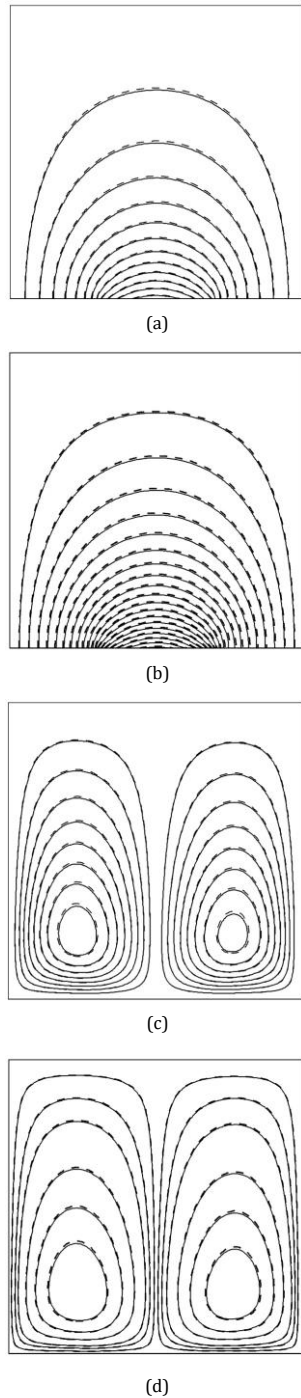
Figure 15. Comparison between contours of temperature (a & b) and streamfunction (c &d) for density ratio of 0.03(a & c) and 0.12(b &d) at $Ra=10^5$, Pr=6.2, $Da = 10^{-4}$, ε = 0.4, reduced order model (solid Line) and CFD data (dashed lines).

In Table **6**, a comparison between the total computational time of CFD simulation and the reduced-order model, which is presented in this study, has been shown. These data show that the cost of computation using the reduced-order model is very less than the CFD simulation approach. But based on data in Table 5, the accuracy of the reduced order model is acceptable compared to the CFD data.

Table 6. Total RMSE of flow and thermal fields

φ	Temperature	Streamfunction	Vorticity
0.03	6.424×10^{-6}	1.937×10^{-6}	6.65×10^{-4}
0.12	1.3271×10^{-5}	2.133×10^{-5}	2.76×10^{-4}

Table 7. Comparison between computational time of CFD and reduced order models

Model	Time (second)	Total Time (second)
CFD	------	640
POD Modes Computations	45	
POD Modes Selection	5	65
Estimation of Flow Field in New Statement	15	

Conclusions

In recent years, considerable research has been made in advancing the state-of-the-art of numerical simulation of Nano-fluid flow in porous media. Some of these works are about the simulation and parametric studying of nanofluid flow especially contains natural convection is discussed in the literature. In this paper, two frameworks have been developed for the simulation of the fluid flow and thermal field containing cu-water nanofluid. In the first, a direct simulation approach is considered while in the second a surrogate model is developed.

This research contributes a POD-based reduced order model for the prediction of the flow and thermal fields and demonstrates its suitability due to the variations of some effective parameters. The POD snapshots method was used for the calculation of the dominant eigenfunctions of flow fields and an order-reduction strategy was used to choose enough modes to reconstruct the reduced order model.

The outcome model is used for the fast prediction of the flow and thermal fields under the effects of variations of some important parameters. The results show that the parametric reduced order model has relatively good accuracy compared to the results obtained from the direct numerical simulation. Also, it is observed that the reduced order model has very small values of errors and its cost of computations is less than 10% compared to direct numerical simulation.

Nomenclature

C_p	Specific heat
g	Gravitational acceleration
k	Thermal conductivity coefficient
K	Permeability of the medium

L	Characteristic length
p	Pressure
t	Time
T	Temperature
$\tilde{T}$	Dimensionless temperature
u	Velocity vector
u	x-component velocity
v	y-component velocity

Greek symbols

α	Thermal diffusivity
β	Thermal expansion coefficient
ρ	Density
φ	Density ratio of nanoparticles
ε	Porosity
κ	Fraction number
μ	Viscosity
ψ	Streamfunction
ω	Vorticity
ν	Kinematic viscosity

Subscripts

c	Cold
D	Darcy (in viscosity description)
f	Fluid
P	Particle
nf	Nano-fluid

Conflicts of Interest

The author declares that there is no conflict of interest regarding the publication of this manuscript. In addition, the authors have entirely observed the ethical issues, including plagiarism, informed consent, misconduct, data fabrication and/or falsification, double publication and/or submission, and redundancy.

References

[1] Eiyad Abu-Nada, Ziyad Masoud, Hakan F. Oztop, Antonio Campo, 2010, Effect of Nanofluid variable properties on natural convection in enclosures, Int. Journal of Thermal Sciences, 49, pp.479–491.

[2] Mefteh Bouhalleb, Hassan Abbassi, 2014, Natural convection of nanofluids in enclosures with low aspect ratios, Int. Journal of hydrogen energy, 39, pp.15275-15286.

[3] Bishwajit Sharma, Basant Kumar, Rabindra Nath Barman, 2018, Numerical investigation of cu-water nanofluid in a differentially heated square cavity with conducting solid square cylinder at center, Int. Journal of Heat and Technology, 36(2), pp.714-722.

[4] M. Izadi, R. Mohebbi, D. Karimi, M. A. Sheremet, 2018, Numerical simulation of natural convection heat transfer inside a $\perp$ shaped cavity filled by a MWCNT-Fe3O4/water hybrid nanofluids using LBM, Chemical Engineering and Processing - Process Intensification, 125, pp. 56-66.

[5] M. Izadi, A. Behzadmehr & M. M. Shahmardan, 2015, Effects of Inclination Angle on Mixed Convection Heat Transfer of a Nanofluid in a Square Cavity, International Journal for Computational Methods in Engineering Science and Mechanics, 16(1), pp.11-21.

[6] M. Izadi, M.M. Shahmardan, A. Behzadmehr, A.M. Rashidi, and A. Amrollahi, 2015, Modeling of Effective Thermal Conductivity and Viscosity of Carbon Structured Nanofluid, Challenges in Nano and Micro Scale Science and Technology, 3(1), pp.1-13.

[7] M. Izadi, M.M. Shahmardan, and A.M. Rashidi, 2013, Study on Thermal and Hydrodynamic Indexes of a Nanofluid Flow in a Micro Heat Sink", Challenges in Nano and Micro Scale Science and Technology, 1(1), pp. 53-63.

[8] M. Izadi, H. M. Alshehri, F. Hosseinzadeh, M. Shokri Rad, M. Bechir Ben Hamida, 2023, Numerical study on forced convection heat transfer of TiO2/water nanofluid flow inside a double-pipe heat exchanger with spindle-shaped turbulators", Engineering Analysis with Boundary Elements, 150, pp. 612-623.

[9] M. Izadi, T. Tayebi, H.M. Alshehri, 2023, Transient magneto-buoyant convection of a magnetizable nanofluid inside a circle sensible storage subjected to double time-dependent thermal sources, Journal of Thermal Analysis and Calorimetry, 148, pp. 8511–8531.

[10] Nazia, S, Seshaiah, B, Sudarsana Reddy, P, Sreedevi, P., 2023, Silver–ethylene glycol and copper–ethylene glycol based thermally radiative nanofluid characteristics between two rotating stretchable disks with modified Fourier heat flux, Heat Transfer, 52, pp.289- 316.

[11] P Sudarsana Reddy, and P Sreedevi, 2021, Flow and heat transfer analysis of carbon nanotubes based nanofluid flow inside a cavity with modified Fourier heat flux, Phys. Scr, 96 055215.

[12] M.R. Aminian, A.R. Miroliaei, and B. Mirzaei Ziapour, 2019, Numerical study of flow and heat transfer characteristics of CuO/H2O nanofluid within a mini tube, Journal of Heat and Mass Transfer Research, 6(1), pp.11-20.

[13] S. Kaviany, 1995, Principles of Heat Transfer in Porous Media, Springer-Verlag, NY.

[14] Ling, X.; Yan, Z.; Liu, Y.; Lu, G. 2021, Transport of nanoparticles in porous media and its effects on the co-existing pollutants, Environmental Pollutants, 283, 117098.

[15] G.C. Bourantas, E.D. Skouras, V.C. Loukopoulos, V.N. Burganos, 2014, Heat transfer and natural convection of nanofluids in porous media, European Journal of Mechanics - B/Fluids, 43, pp. 45-56.

[16] Prabir Barman and PS Rao, 2022, Natural convection of nanofluids in a wavy porous cavity, Proceedings of the Institution of Mechanical Engineers, Part C: Journal of Mechanical Engineering Science, 236(7), pp. 3847-3863.

[17] Basil Mahdi Al-Srayyih, Shian Gao, and Salam Hadi Hussain , 2019, Natural convection flow of a hybrid nanofluid in a square enclosure partially filled with a porous medium using a thermal non-equilibrium model, Physics of Fluids, 31, 043609.

[18] Z. A. S. Raizah and A. M. Aly, 2021, Natural convection in an h-shaped porous enclosure filled with a nanofluid, Computers, Materials & Continua, 66(3), pp. 3233–3251.

[19] S.A.M. Mehryan, M. Ghalambaz, A. J. Chamkha, M. Izadi, 2020, Numerical study on natural convection of Ag–MgO hybrid/water nanofluid inside a porous enclosure: A local thermal non-equilibrium model, Powder Technology, 367, pp. 443-455.

[21] M. Izadi, B. Bastani and M. A. Sheremet, 2020, Numerical simulation of thermogravitational energy transport of a hybrid nanoliquid within a porous triangular chamber using the two-phase mixture approach, Advanced Powder Technology, Vol. 31(6), pp. 2493-2504.

[22] H. Sajjadi, A. A. Delouei, R. Mohebbi, M. Izadi, and S. Succi, 2020, Natural convection heat transfer in a porous cavity with sinusoidal temperature distribution using Cu/Water nanofluid: Double MRT Lattice Boltzmann Method, Communications in Computational Physics, 29(1), pp.292-318.

[23] M. Izadi, R. Mohebbi, A. A. Delouei, H. Sajjadi, 2019, Natural convection of a magnetizable hybrid nanofluid inside a porous enclosure subjected to two variable magnetic fields, International Journal of Mechanical Sciences, 151, pp.154-169.

[24] M. Izadi, B. Alshuraiaan, A. Hajjar, M. A. Sheremet, M. B. Ben Hamida, 2023, Free convection of nanofluids in a porous sensible heat storage unit: Combined effect of time periodic heating and external magnetic field, International Journal of Thermal Sciences, 192 part A.

[25] P. Holmes, J. L. Lumley, G. Berkooz, 1996, Turbulence coherent structures, dynamical systems and symmetry, Cambridge, UK, Cambridge University Press.

[26] Rathinam, Muruhan and Petzold, Linda., 2023, A New Look at Proper Orthogonal Decomposition, SIAM J. Numerical Analysis, 41, pp.1893-1925.

[27] Feng, J. W., Cen, S., Li, C. F., and Owen, D. R. J., 2015, Statistical reconstruction and Karhunen–Loève expansion for multiphase random media, Int. Journal of Numerical Methods in Engineering, 105, pp.3– 32.

[28] Holmes P.J., Lumley J.L., Berkooz G., Mattingly J.C., Wittenberg R. W., 1997, Low-dimensional models of coherent structures in turbulence, Physics Reports, 287(4), pp. 337-384.

[28] Holmes P.J., Lumley J.L., Berkooz G., Mattingly J.C., Wittenberg R. W., 1997, Low-dimensional models of coherent structures in turbulence, Physics Reports, 287(4), pp. 337-384.

[29] Smith, T. R., Moehlis, J., and Holmes, P., 2004, Low-Dimensional Modeling of Turbulence Using the Proper Orthogonal Decomposition: A tutorial", Kluwer Academic, Boston.

[30] L. Sirovich, M. Kirby, 1987, Low-dimensional procedure for the characterization of human faces, J. Optical Society America, 4(3), 519–24.

[31] T. Lieu, C. Farhat, 2005, Adaptation of POD-based aeroelastic ROMs for varying Mach number and angle of attack: Application to a complete F16 configuration, AIAA Journal.

[32] Li, J., Zhang, T., Sun, S. and Yu, B., 2019, Numerical investigation of the POD reduced-order model for fast predictions of two-phase flows in porous media", International Journal of Numerical Methods for Heat & Fluid Flow, 29(11), pp. 4167-4204.

[33] Thomas A. Brenner, Raymond L. Fontenot, Paul G.A. Cizmas, Thomas J. O'Brien, Ronald W. Breault, 2012, A reduced-order model for heat transfer in multiphase flow and practical aspects of the proper orthogonal decomposition, Computers & Chemical Engineering, 43, pp. 68-80.

[34] Alexandra Tallet, Cyrille Allery & Cédric Leblond, 2016, Optimal flow control using a POD-based reduced-order model, Numerical Heat Transfer, Part B: Fundamentals, Vol.70(1), pp.1-24.

[35] Li, S., Li, W., & Noack, B., 2022, Machine-learned control-oriented flow estimation for multi-actuator multi-sensor systems exemplified for the fluidic pinball, Journal of Fluid Mechanics, 952, A36.

[36] J. R. Connell, D. Kulasiri, 2007, Computational modeling of turbulent velocity structures for an open channel flow using Karhunen-Loeve expansion, Lincoln University.

[37] T. Bui-Thanh, M. Damodaran, K. E. Willcox, 2004, Aerodynamic data reconstruction and inverse design using proper orthogonal decomposition, AIAA Journal.

[38] R. Bourguet, M. Braza, A. Dervieux, 2011, Reduced-Order modeling of transonic flows around an airfoil submitted to small deformations, Journal of Computational Physics, 230, 159–184.

[39] M.K. Moayyedi, M. Najafbeygi, 2018, A high fidelity cost efficient tensorial method based on combined POD-HOSVD reduced order model of flow field, European Journal of Computational Mechanics, 27(4), 342–366.

[40] Zhendong Luo, 2015, Proper Orthogonal Decomposition-based Reduced-order Stabilized Mixed Finite Volume Element Extrapolating Model for the Non-stationary Incompressible Boussinesq equations, Journal of Mathematical Analysis and Applications, 425(1), pp. 259-280.

[41] M.K. Moayyedi, 2017, Numerical simulation and reduced order modeling of mass transfer due to natural convection based on coupling between temperature and contaminant, Sharif Journal of Mechanical Engineering, 33.3(2), pp.43-52.

[42] M. K. Moayyedi, F. Sabaghzadeghan, 2021, Development of parametric and time dependent reduced order model for diffusion and convection-diffusion problems based on proper orthogonal decomposition method", Amirkabir Journal of Mechanical Engineering, 53(7), pp. 4241-4260.